November 8, 2000

A Radio Study of the Evolution of Spatial Structure of an Active Region and Flare Productivity

M. R. Kundu, S. M. White,

Astronomy Department, University of Maryland, College Park, MD 20742

K. Shibasaki

Nobeyama Radio Observatory, NAO, Minamisaku, Nagano 384-13, Japan

J.-P. Raulin,

CRAAE, Instituto Presbiteriano Mackenzie, Rua de Consolação, 896, 01302–000 São Paulo, SP, Brazil

ABSTRACT

We present the results of a radio study of the evolution of an active region through its flare productivity. The radio study was carried out with data obtained by the Nobeyama Radio Heliograph (NoRH) at 17 GHz. We chose the active region AR 7515 which appeared at the east limb on May 23, 1993 and then evolved during its passage across the disk. We followed its evolution until June 2. This region produced many small flares. We consider this region to be a typical active region in the sense that it did not produce any large flare, but a large number of weak flares. We investigate the optical and magnetic development of the region and show how this affects the locations of the flaring activity. We discuss a number of events in detail in order to investigate the roles of nonthermal and thermal radio emission in the flares. The nonthermal gyrosynchrotron emission generally occurs in regions of strong magnetic fields, is generally circularly polarized and often varies rapidly in time. On the other hand, gradual radio components tend to be thermal and only weakly polarized if at all. An interesting aspect of the evolution of the flares in this region is that many of the flares in the early phase of the evolution show strong but brief nonthermal radio emission in the impulsive phase followed by gradual thermal emission, whereas in the last 3 days more gradual events without a strong spike of radio emission in the impulsive phase tend to be seen. Correspondingly, the flare images suggest that the radio sources are more compact during the early phases and more extended in the last half of the period covered. The most dominant component of the preflare region is often not the component which undergoes immediate flaring. Sometimes a number of components in the preflare region participate in the flare process together. We speculate that these component sources are unresolved compact bipolar loops which flare in sequence. Loop–loop interactions occurring at many different sites at the same time seems to be a less plausible explanation of these events.

Subject headings: Sun: flares, radio radiation, corona

1. INTRODUCTION

Observation of the evolution of an active region is important for understanding which of its many properties is critical for its ultimate flare productivity. Such observations at short centimeter wavelengths are important because these radio emissions originate from the lower corona where the solar flare energy release process is believed to take place. We know that certain evolutionary properties of active regions have their signatures at the photospheric level. Thus, it is clear from vector magnetograms of active regions that magnetic shear is critically important for a flare to take place (e.g., Hagyard et al. 1986). From high spatial resolution microwave observations using the VLA, Kundu et al. (1982, 1984) showed that the emergence of a new region interacting with a pre-existing region can lead to the occurrence of a flare. More recently, using the Yohkoh/SXT data, Hanaoka (1994) carried out studies on flare productivity of active regions/coronal loops. Thus, Hanaoka reported a case in which about 24 hours before a flare, coronal loops were weakly sheared; subsequently a rapid spot motion with a velocity of 0.25 km s^{-1} was observed, which resulted in a sheared structure of the coronal loops, and a flare occurred at the intersection of the sheared loops. This observation showed that the energy build up in the corona could be caused by increasing shear of magnetic field due to photospheric flow and that the flare resulted from the interaction of sheared coronal loops. In order to prove the role of shear in these observations, Hanoaka had to rely on SXT optical pictures obtained with glass filters imaged on a CCD along with SXT X-ray images showing the coronal loops.

It is clear that observations in various spectral domains - optical, X-ray and radio - indicate that solar flares occur in complexes of two or more magnetic loops. The existence of two or more magnetic loops suggests that flares are often caused by interactions between the loops. Interactions between newly emerging flux and the overlying magnetic field have been inferred as the cause of flares (e.g., Zirin 1983, Kurokawa 1989). In the microwave radio domain, the VLA observation of a flare at 2 cm was interpreted as due to the appearance of a new region; the implication was that the flare resulted from the interaction of a newly appearing region with the pre-existing region/magnetic field (Kundu & Shevgaonkar 1985). More recently, Yohkoh/SXT imaging data have revealed that interactions between coronal loops can lead to both flares and microflares (e.g., Hanaoka 1994, Shimizu et al. 1994). Using H-alpha and magnetogram observations of flares, Mandrini et al. (1991) and Demoulin et al. (1993) also concluded that the interaction of bipoles (or loops) is essential for triggering a flare. All these observations of interaction between loops as a causative element in the production of solar flares is in accord with the general ideas inherent in solar flare models as developed by Heyvaerts et al. (1977). On the other hand there is increasing evidence that many simple weak flares can originate from compact bipolar flaring loops (see Kundu et al. 2000b) without any interaction with other loops.

Hanoaka's primary observations were carried out with the Nobeyama Radio Heliograph (NoRH) at 17 GHz. Subsequent studies by Hanaoka (1996, 1997) provided more details on the interaction between coronal loops as the primary factor which influences the production of flares: (1) interaction between an emerging loop and an overlying loop referred to as double-loop interaction by Hanaoka (c.f. Kundu et al. 1982 & Kundu et al. 1984); (2) interaction of a small emerging loop near the foot points of a pre-existing large coronal loop; according to Hanoaka, brightening in the small loop preceded the brightening in the large loop which is the main flare site. Indeed, Hanoaka (1996, 1997) analyzed two sets of flare-producing active regions where emerging flux appeared, using Yohkoh-SXT and NoRH 17 GHz imaging data along with available optical and magnetic field data. He showed that emerging flux appearing near a spot and interacting with an overlying loop could produce flares and microflares. The location of the emerging flux appeared to be the main flare site, where both X-ray and 17 GHz brightenings occurred. Further, there was an additional microwave brightening at a remote region ($\sim 10^5$ km away). The two microwave sources were connected by a large soft X-ray loop. He characterized this "double-loop" topology as an important magnetic configuration in an active region for triggering flares. In fact, Hanoaka went one step further by characterizing the double-loop configuration as a three-legged structure, because at the main flare site the microwave and hard X-ray sources consisted of two foot points with distinctive polarization behavior in microwaves. Such remote brightenings in microwaves were observed previously by Nakajima et al. (1985) and Kundu et al. (1983). However, the case for interaction between emerging flux and an overlying loop at the main flare was not made in these observations.

In this paper, we study the evolution of spatial structure of an active region (AR 7515) over a period of 10 days, and how the region undergoes structural changes in relation to flare productivity. We use 17 GHz imaging data from the Nobeyama radioheliograph for this study.

This region appeared at the east limb on May 23, 1993. We followed its evolution until June 2. This region produced many small flares. We study the magnetic and structural topology of the active region components as observed at 17 GHz by the Nobeyama Radio Heliograph (NoRH) and Yohkoh/SXT to find their effects on flare production. We investigate the spatial structure of the flaring region from 17 GHz and SXT maps during various times of the flare phenomenon, to understand the difference in the flaring region spatial structure during the preflare, impulsive and decay phases. We observed over 30 flares at 17 GHz originating from the same AR over the period May 23 to June 2, 1993. We have studied the behavior of the active region in relation to flare productivity.

We will be concerned primarily with a study of the active region radio maps during the preflare stage, the main flaring phase and in the post flare phase, and from the locations of the burst emission sources in various phases with respect to the component sources in the preflare phase, address the issue of whether we see compact bipolar flaring loops or interaction between loops in the radio images.

2. NOBEYAMA RADIO HELIOGRAPH

The microwave radio images used in this paper were obtained with the Nobeyama Radio Heliograph (NoRH) at 17 GHz. The radio observations at 17 GHz were made with a spatial resolution of $15''$ and a temporal resolution of 1 s. The NoRH consists of 84 paraboloidal antennas, each antenna being of 80 cm in diameter. They are located in a T-shaped array (E-W and N-S). The NoRH records both right-handed and left-handed circular polarization and has a field of view of $40'$ covering the entire Sun. The NoRH has a dynamic range of better than 25 db (Koshiishi et al. 1994) and in the snapshot mode (1 sec), it has a sensitivity of 400 K (4.4 msfu for a point source). The NoRH has been used mainly for the study of intense bright phenomena such as active regions including sunspot-associated microwave sources, or high contrast flares, eruptive prominences, etc. (Enome et al. 1994; Shibasaki et al. 1994). The study of weaker solar phenomena at 17 GHz has recently been possible due to the development of new software by Koshiishi (1996) which permits much higher dynamic range and better image quality for analysis of low brightness solar phenomena. We produced full disk maps at 17 GHz using the earlier Hanoaka program as well as the recently developed programs by Koshiishi (1996) and Fujiki (1997). The Fujiki program is more appropriate for us, because it gives a much cleaner beam with the theoretical resolution of $10''$. We show two sets of data for the active region: (1) spatial structure; (2) intensity-time plots. The time profiles of the bursts shown are the correlated amplitude of the 350 longest baselines of the array versus time. We also show the flux values computed from images at selected times.

The correlation amplitude is not sensitive to large scale features, whereas the map-computed values give the whole flux. The field of view of each image is about $5' \times 5'$. Polarization data are available; they were used in our analysis but not always shown.

In specific event analyses we will also refer to microwave spectral information acquired with the radio polarimeters of Toyokawa Observatory, kindly provided by Nobeyama Radio Observatory. These data consist of 1-second resolution full–disk fluxes at 1.0, 2.0, 3.75 & 9.4 GHz with a sensitivity of order 1 – 2 sfu, and by comparison with the 17 GHz radioheliograph fluxes they allow us to determine the location of the radio spectral peak (i.e., the frequency at which the radio flux is maximum). At frequencies above the spectral peak the radio emission will be predominantly optically thin.

3. MAGNETIC EVOLUTION

Figure 1 shows the evolution of AR 7515 in white light and magnetogram data and in soft X-rays from May 25 to June 3. At the east limb AR 7515 was dominated by a large negative-polarity spot displaced northwards of a number of small spots of mixed polarity in the trailing part of the region. Soft X–ray emission is brightest in the trailing part of the region on May 26, but by May 27 a strong X–ray bridge betwen the leading and trailing parts of the group has developed. As the region approaches central meridian, the foremost spot in the southern trailing region grows into a double spot and moves forward relative to the leading northern spot (May 29). Bright X–ray loops connect the evolving southern leading spot to the trailing part of the region but not to the northern leading spot. By May 30, the southern leading spot is larger than the northern leading spot and almost at the same longitude. Simultaneously an intense region of negative polarity erupts amongst the dominant positive polarity at the rear of the active region, peaks on May 31 but vanishes by the next day. There is now bright X–ray emission lying between the two leading negative–polarity spots, but as there is no obvious positive polarity located near them these X–ray loops must connect back to the positive polarity in the trailing part of the region. As the region proceeds towards the west limb, the northern leading spot shrinks while the southern leading spot remains large and is abruptly joined by another negative-polarity spot just to the east on June 2. By June 3 the magnetic structure of the region has simplified (little mixed polarity) although impressive spots are still present. In X–rays we see generally long loops connecting the leading and trailing parts of the region.

The locations of optical flares on each day taken from Solar Geophysical Data are shown as crosses on Figure 1 (positions rotated to the times of the optical images). On May 26-29, flares mostly occur in the trailing part of the region; on May 30 and 31, as the southern leading spot moves forward, the flares occur around the two leading spots; on June 1 and 2, the flares move back to the trailing part of the region where the new large spot emerges; and on June 3, with the northern leading spot disintegrating, the flares again occur between it and the other large spots.

Figure 2 shows the GOES 1.5 – 10 keV soft X–ray light curves during Japanese daylight time for the period investigated. Many of the X–ray flares during this period occurred in AR 7515, and those whose radio emission we have mapped are marked on the figure. Note the presence of both short–duration and longer–duration soft X–ray events on this figure: for example, a very impulsive soft X–ray event is seen at 02:00 UT on May 26, while several long–duration events occur on May 30. Most of the flares are GOES C–class events; a few just exceed the GOES M–class threshhold.

Figures 3 and 4 summarize the radio burst activity from this region observed at NoRH at 17 GHz. As mentioned earlier, we observed about 3 dozen bursts at 17 GHz during the period May 25 to June 2, 1993: the time profile of 17 GHz radio flux from small spatial scales derived from long baselines of the radioheliograph is shown in Figure 3, which may be compared directly with the soft X–ray light curves in Figure 2. The radio bursts are mostly weak (1 to tens of SFU), although we note that Figure 3 does not show the total flux from each burst since any bursts covering a large solid angle will have their fluxes underestimated in Figure 3.

Figure 4 shows maps of 28 separate radio bursts over 9 days. In each panel the date and time of the burst are labelled: solid thin grey contours show a preflare image of the active region radio emission, thick black contours (on some panels) show preflare circularly polarized flux when the degree of polarization exceeds 30%, while the greyscale shows the location of the radio burst emission after preflare subtraction. Thus the panels show both the evolution of the active region component of the radio emission as well as the distribution of radio bursts as the region rotates across the solar disk. The resolution of the radio images is $15''$ - $20''$. The flare times plotted are chosen to be representative of the flare morphology.

On May 25 & 26, the region is near the east limb and the active region emission shows free–free emission from loops extending tens of arcseconds above the photosphere. For most of the period shown there is no strong 17 GHz gyroresonance source present in the active region (such a source would require 2000 G magnetic field strengths in the solar corona: they are easily recognized by the strong circular polarization which they usually produce). One may be seen in the center of the active region on May 27, over a positive–polarity spot located there, but it does not last more than 1 day. On May 28 a new gyroresonance source appears over the southern sunspot which moves out ahead of the rest of the active region. Significant circular polarization remains above the southernmost of the large leading sunspots for much of the period, whereas no strong gyroresonance source is seen above the northern large leading sunspot.

As a general statement, the bulk of the preflare radio emission is similar in appearance to the soft X–ray emission seen in Figure 1, which is to be expected since the radio emission away from sunspots is likely to be free–free emission. Some exceptions may be found when the preflare radio map clearly contains residual emission from a prior flare, such as the maps at 23:01 UT on May 28 and 06:48 on May 30. The general elongation of the region remarked upon in Figure 1 is also seen in Figure 4: with the leading northern sunspot apparently playing little role in the radio appearance of the region, the dominant influence is the forward motion of the southern leading spots which can first be seen as a flare at the western edge of the radio source on May 27 (01:06 UT) and then in the evolution of the active region emission in the radio images on May 28: a distinct compact source associated with the moving sunspot is seen to the west of the main radio source from 0 UT onwards, and is the site of several flares. The separation of the leading radio source from the main radio source is maintained until the end of May; by June 1 & 2 there is no longer any separation observed. Of 11 radio bursts on May 28 – 30, 7 show emission associated with this leading-spot source. Most of the later radio bursts do not occur at the western edge of the region, however.

4. 17 GHz FLARES IN AR 7515

Inspection of Figure 3 reveals that many, but not all, of the radio events in AR 7515 contain a brief impulsive spike at the onset of the impulsive phase, frequently followed by a longer–duration emission which resembles the soft X–ray time profile. We identify the brief impulsive emission as a nonthermal impulsive phase, based on many prior studies in which such time profiles have a nonthermal spectrum (Bastian et al. 1998). This is confirmed for our events by inspection of the radio spectrum when available. The longer duration phase is often due to thermal emission from hot plasma due to heating of the chromosphere by the nonthermal electrons. This is the same plasma which produces the soft X–rays in the GOES time profile. Other events, such as the first three events on May 30, show correlation–plot time profiles which cannot be interpreted simply, but which can be understood better when the total flux time profiles are used and spatially analyzed. We investigate the characteristics of a selection of these events intended to represent the observed flares in more detail in this section. Event numbers given below refer to the labels on Figures 2 & 3 for each day. The large events at 02:00 UT on May 28 (a simple bipolar nonthermal 17 GHz source followed by a thermal decay phase) and 06:48 UT on May 30 (similarly simple impulsive time profile but spatially more complex, with a highly polarized source at one end and unpolarized emission extending $100''$ to the east) have already been discussed in detail by Kundu et al. (1995).

4.1. May 26, 00:18 UT; event 2

This event has a time profile consisting of a simple impulsive spike followed by a long–duration gradual component. Images of the event (Figure 5) show two components: a north–western feature which is the source of the impulsive spike and which is weakly polarized; and a south–eastern component which dominates the gradual phase and is essentially unpolarized. This event is too weak to be detected by the Toyokawa polarimeters, so we cannot determine the radio spectrum, but the time profile at 17 GHz is consistent with a nonthermal impulsive peak followed by a thermal component matching the GOES profile. The images indicate that these two components come from different locations.

4.2. May 26, 02:10 UT; event 4

This event is very similar to the previous event discussed: the location and details are nearly identical. The 17 GHz time profile for this event shows a rise over about 1 minute followed by a very gradual decay. The event is not detected by the Toyokawa polarimeters. Again the similarity of the radio decay phase and the GOES light curve suggest that the long–duration component is a thermal decay phase. Figure 6 shows that the images of this event may be separated into the same north–western impulsive and weakly polarized component and south–eastern, longer-lasting unpolarized component observed in the previous flare. One interesting difference is that while they are nearly identical in GOES flux and in the strength of the nonthermal 17 GHz emission, the earlier event shows a radio flux in the thermal decay phase which is about twice the flux seen in this event. Note also that the two components are connected by lower–level contours, giving the appearance of a loop–like structure at 02:14 UT.

4.3. May 27, 00:55 UT; event 2

This event has no obvious impulsive phase, but rather a long gradual rise featuring several distinct peaks. The soft X–rays during this period also show two peaks, suggesting two energy releases. In this case the images of the flare (Figure 7) show two components at 17 GHz, but both have gradual time profiles and are weakly (positively) circularly polarized.

They do however peak at different times. The radio flux data are consistent with a flat spectrum from 9 to 17 GHz, suggesting that there is no nonthermal emission in this event.

The dominant sense of circular polarization is right handed, corresponding to upgoing (positive) magnetic field. A positively–polarized gyroresonance source exists over the positive spot in the center of the active region on this day, as shown in the V maps; this source does not seem to vary greatly in V during the flare (lower row of panels in Fig. 7). The elongated south–western source (light curve in the upper row of Fig. 7) seems to be associated with downgoing magnetic flux visible just south of the central sunspot (and just east of the negative southern spot which subsequently detaches itself).

4.4. May 28, 01:05 UT; event 2

This event is again dominated by a compact polarized component at onset, but during decay the radio emission comes from a much larger region which is unpolarized (Figure 8). There is no significant detection in the Toyokawa data. The gradual nature of the 17 GHz profile and its similarity to the GOES profile suggest a thermal origin. The location of this event (see Figures 1 & 4) is over the negative southern spot which has commenced its westward movement, although no gyroresonance source is present in the preflare images.

4.5. May 28, 03:00 UT; event 4

This is a large extended event for which we plot time profiles at three separate locations (Figure 9). Prior to the main impulsive phase at about 03:00 UT, a weak negatively–polarized gyroresonance source is present at the leading edge of the region (over the negative southern spot) and a weak brightening is seen in a source in the center of the region (lying in the leftmost box in the upper left panel of Fig. 9). This source fades prior to 03:00 UT and then brightens again in the decay phase (upper right panel). The gyroresonance source (middle row of panels in Fig. 9) dominates in the impulsive phase, with significant negative polarization, and then decays. The region to the north of the gyroresonance source (lower row of panels in Fig. 9) dominates the decay phase and is very weakly positively polarized.

This event shows a very strong brief burst at 1.00 GHz right at flare onset which is presumably due to some coherent emission process. No emission is seen at any other frequency at this time (02:52:30). The lower frequencies (2.0 & 3.75 GHz) start to rise at this time, with the higher frequencies (9.4 & 17 GHz) lagging by several minutes. The radio spectrum appears to be nonthermal during the peak at 03:00 UT, but is probably thermal thereafter.

4.6. May 30, 04:00 UT; event 2

This is one of the larger radio events with quite a long duration in both radio and soft X–rays. The radio images show three sources with quite distinct time evolutions (Figure 10). The lower source, associated with the preflare gyroresonance source over the southern negatively polarized spot, is highly polarized throughout and shows several peaks during the 5 minute period starting at 04:05 UT (upper panels of Fig. 10). The two northern sources both appear well after emission starts in the southern source, and both show more gradual, longer–lasting time profiles. The north–eastern source (lower row of panels), which peaks later than the other two sources, is clearly extended and eventually appears to be a loop connecting to the southern source. The north–western source (middle row of panels) appears to lie close to the northern negative leading spot, which is generally inactive in these events. No steady gyroresonance source is ever seen over this source. The flare emission at this location in this event is around 40% polarized, while that at the main source over the negative southern sunspot is about 50% polarized. These values are too high for the emission plausibly to be from soft–X–ray loops emitting bremsstrahlung during the decay phase. The overall radio spectrum appears to be nonthermal from 04:05 – 04:10 UT, but the total flux is dominated by the southern source, which must therefore be nonthermal, while the northern sources are weaker and their radio spectra cannot be determined. The polarization of the north–eastern source is low, but this may either be nonthermal gyrosynchrotron emission from weaker magnetic fields, or thermal bremsstrahlung emission.

4.7. May 30, 05:10 UT; event 3

This is another large and complex event. Radio emission commences at around 05:06 UT and rises very gradually. A period of impulsive spiky emission (at 2.00 and 17 GHz, but apparently not at 9.4 GHz) takes place from 05:18 to 05:23 UT. The GOES light curve shows a long event with two peaks.

The 17 GHz images show that this event occurred in a location similar to that of the previous event, and initially the same three sources are involved. Subsequently the burst emission expands to cover a much larger area. The light curves for different source regions (Figure 11) show that the spiky emission emerges from the vicinity of the preflare gyroresonance source over the negative southern leading spot (upper row of panels) and is again very highly polarized (40%). The north–eastern source (middle row of panels) is bright but has a fairly gradual time profile peaking at 05:23 UT, while the second northern source plotted (lower row of panels in Fig. 11; note that this location is to the east of the north–western source plotted in Fig. 10) also has a gradual time profile but with a much later peak (05:33 UT). The radio spectrum suggest that the spiky emission is nonthermal, but that emission after 05:23 is largely thermal. This suggests a scenario similar to a double ribbon event, in which the initial nonthermal energy release occurs in a confined location but subsequently soft X–ray–emitting loops spread to cover a much larger area. We speculate that such loops are responsible for the northern sources whose time profiles are plotted (middle and lower rows of panels) via bremsstrahlung emission. The north–western source over the northern leading spot, whose time profile is not plotted in Fig. 11, again shows $\sim$ 40% polarized emission peaking at 05:35 UT as in the adjacent source plotted in the bottom row of panels in Fig. 11, which suggests that the latter source may be emitting nonthermal radiation. The radio spectra of this event are difficult to interpret because of the presence of spiky emission at some frequencies but not others.

4.8. June 01, 23:05 UT; event 1

Another weak event which was barely detected at 9.4 GHz, the time profile shows a single main peak with quite a rapid rise and lasting several minutes. The event occurs at the trailing end of the region (see Fig. 4) and the 17 GHz images (Figure 12) again show several sources. The two main sources appear to be connected and may represent the two ends of a single loop; they have very similar time profiles. One end is significantly positively polarized. We also plot the time profile of a large low–surface–brightness feature at the western end of the region which appears to brighten later; this source might not be related to the main flare, and is the site of a negtively–polarized steady gyroresonance source, apparently over one of the two large southern negative sunspots at the front of the active region on June 2 (Figure 1). The radio spectrum of this event appears to be nonthermal in the impulsive phase.

4.9. June 02, 02:57 UT; event 2

By contrast with the preceding event (Fig. 12) four hours earlier, this event brightens initially near the leading edge of the active region and then spreads towards the center of the region. The initial brightening lies over the leading southern sunspot, and this location shows highly negatively polarized emission (Figure 13, top panels). At the trailing end of the apparent loop structure in the early images lies a weakly positively polarized source, implying that indeed an extended loop is seen connecting sites $80''$ apart. During the extended thermal decay phase the polarized emission near the leading sunspot weakens while the emission to the north-east remains strong but unpolarized.

5. DISCUSSION AND CONCLUSIONS

We have performed a morphological study of the evolution of spatial structure of an active region at 17 GHz over a 10–day period in relation to its flare productivity. This was an active region which produced only weak activity, that is, weak bursts at 17 GHz. It produced about 3 dozen bursts at 17 GHz, but they were all weak - none bigger than ~ 10 sfu, with the exception of two spiky bursts which were stronger (≥ 50 sfu) and which could be mapped by Yohkoh-HXT in the L and M1 channels. These two bursts observed on 1993 May 28 and May 30 have been described by Kundu et al. (1995). We consider this region to be a typical active region in the sense that it did not produce any large flare, but a large number of weak flares. Thus an investigation of its flare productivity may be valuable as an example of non–extreme behaviour.

The analyses of individual events in the preceding section show that, even for a single active region, radio flares may vary greatly in the relative importance of nonthermal gyrosynchrotron emission (usually dominant for brief periods in the impulsive phase) and thermal bremsstrahlung emission (typically dominant in the decay phase, and in gradual events). An interesting aspect of the evolution of the flares in this region is that the proportion of flares which show strong but brief nonthermal radio emission in the impulsive phase followed by gradual thermal emission (e.g., event 3 on May 28 in Fig. 3) is large while the region is young, and much lower in the last 3 days when more gradual events without a strong spike of radio emission in the impulsive phase tend to be seen. Correspondingly, the flare images in Fig. 4 suggest that the radio sources are more compact while the active region is young, and more extended in the last half of the period covered.

Not surprisingly, most of the strongly circularly polarized flare radio emission could be identified with sources close to strong magnetic fields in the photosphere. None of the radio sources with gradual time profiles were strongly polarized; conversely, the polarized sources occasionally showed rapidly varying emission not seen elsewhere in the flare sources.

From our study of the evolution of spatial structure of an active region in relation to flare activity, we can make several conclusions . These are listed below.

1) Because of the relatively poor resolution ($\geq 15''$) of the radio images, the preflare region often appears as a complex of several unresolved component sources. One or the other of these pre-existing component sources can suddenly (in a few minutes time) flare up, leading to increased brightening. However, the most dominant component of the preflare complex is very often not the one which will undergo immediate flaring, although at some point in the life time of the preflare region, the brightest component may produce a flare.

2) Based on early low–resolution maps of solar microwave flares, it had been thought

that radio bursts occur at the locations of peaks in the preflare active region radio emission (Pick 1961; Kundu 1965). These observations, and other observations, e.g., from the VLA, have shown that while this is often true at the arcminute level, it is not the case when images at arcsecond resolution are available, and indeed we do not expect it to be the case at 17 GHz: the radio peak in the preflare active region will occur in a gyroresonance source usually over sunspot, or if no such source is present in a region then the peak will occur where bremsstrahlung is brightest, which should coincide with the X–ray peak. The statement that the radio flare does not usually coincide with the brightest preflare emission amounts to saying that flares do not usually occur over the umbrae of large sunspots, or in the brightest X–ray loop present in a region prior to the flare.

3) Although many events have multiple sources, clear examples in which we see a loop with two oppositely–polarized footpoints in the impulsive phase (such as Figure 13) are rare. More often we see the two footpoints of a flaring loop rather than the entire loop in the impulsive phase (e.g., Figs. 5, 7, 10). However, the loop may appear clearly in the post–flare phase due to the filling of the loop with hot plasma emitting bremsstrahlung emission which is weakly polarized or unpolarized (Figs. 7, 8, 9, 11).

4) In general, when there are two component sources, the one responsible for burst emission with a sharp rise phase is polarized, whereas the one responsible for gradual emission is unpolarized.

5) Generally, all bursts with spiky (narrow) time profiles originate from a compact polarized region. Based on other studies (Kundu et al. 2000a,b), such sources may prove to be unresolved compact bipolar flaring loops. When the polarization appears unipolar at low spatial resolution the bipolar loop is asymmetric with different magnetic fields at its foot points.

6) The existence of a number of component sources is dramatically illustrated when the flaring region consists of several sources, all of which participate in the flare (e.g., Figs. 9, 10, 11). These sources may be compact unresolved bipolar loops, in which case they must be flaring in sequence due to some invisible triggering disturbance, or they may be due to loop–loop interactions, which would require both the simultaneous presence of a number of sites where such interactions can take place as well as a triggering disturbance. We do not find any clear examples of loop–loop interaction events similar to those studied by Hanaoka (1996, 1997) and Nishio et al. (1997), indicating either that such events are not common or (more plausibly) that they are not always easily identifiable in data with limited resolution such as these, since the presence of two loops is not always easy to discern, particularly in spatially small events.

Acknowledgments

This research at Maryland was supported by NSF grants ATM 96–12738, ATM 99–90809 and INT–98–19917, and NASA grants NAG 5–8192 and NAG 5–7901.

REFERENCES

Bastian, T. S., Benz, A. O., & Gary, D. E. 1998, Ann. Rev. Astron. Astrophys., 36, 131

Demoulin, P., Van Driel-Gesztelyi, L., Schmieder, B., Henoux, J.-C., Csepura, G., & Hagyard, M. 1993, Astron. Astrophys., 271, 292

Enome, S., Nakajima, H., Shibasaki, K., Nishio, M., Takano, T., Hanaoka, Y., Torii, C., Shiomi, Y., Sekiguchi, H., , Bushimata, T., Kawashima, S., Shinohara, N., Irimajiri, Y., Koshiishi, H., Choi, Y.-S., Sakai, J., Takahashi, M., Takakura, T., Sakao, T., & Kosugi, T. 1994, Publ. Astron. Soc. Japan, 46, L27

Fujiki, H. 1997, Ph. D. Thesis (Japan: Graduate University of Advanced Studies)

Hagyard, M., Chapman, G., de Loach, A., Gary, A., Gaizauskas, V., Jones, H., Karpen, J., Martres, M., Porter, J., Schmieder, B., Smith, J., & Toomre, J. 1986, in Energetic Phenomena on the Sun (Proceedings of the Solar Maximum Mission Workshop, chapter 1), ed. M. R. Kundu, B. E. Woodgate, & E. J. Schmahl, 1

Hanaoka, Y. 1994, Astrophys. J. (Lett.), 420, L37

—. 1996, Solar Phys., 165, 275

—. 1997, Solar Phys., 173, 319

Heyvaerts, J., Priest, E. R., & Rust, D. M. 1977, Astrophys. J., 216, 123

Koshiishi, H. 1996, Ph. D. Thesis (Tokyo: The University of Tokyo)

Koshiishi, H., Enome, S., Nakajima, H., Shibasaki, K., Nishio, M., Takano, T., Hanaoka, Y., Torii, C., Sekiguchi, H., Kawashima, S., Bushimata, T., Shinohara, N., Irimajiri, Y., & Shiomi, Y. 1994, Publ. Astron. Soc. Japan, 46, L33

Kundu, M. R. 1965, Solar Radio Astronomy, 1st edn. (New York: Interscience Publishers)

Kundu, M. R., Machado, M. E., Erskine, F. T., Rovira, M. G., & Schmahl, E. J. 1984, Astron. Astrophys., 132, 241

Kundu, M. R., Nitta, N., White, S. M., Shibasaki, K., Enome, S., Sakao, T., Kosugi, T., & Sakurai, T. 1995, Astrophys. J., 454, 522

Kundu, M. R., Rust, D. M., & Bobrowsky, M. 1983, Astrophys. J., 265, 1084

Kundu, M. R., Schmahl, E. J., Velusamy, T., & Vlahos, L. 1982, Astron. Astrophys., 108, 188

Kundu, M. R. & Shevgaonkar, R. K. 1985, Astrophys. J., 291, 860

Kundu, M. R., White, S. M., Shibasaki, K., & Sakurai, T. 2000a, Astrophys. J., in press

Kundu, M. R., White, S. M., Shibasaki, K., Sakurai, T., & Grechnev, V. V. 2000b, Astrophys. J., in press

Kurokawa, H. 1989, Space Sci. Revs., 51, 49

Mandrini, C. H., Demoulin, P., Henoux, J.-C., & Machado, M. E. 1991, Astron. Astrophys., 250, 54

Nakajima, H., Dennis, B. R., Hoyng, P., Nelson, G., Kosugi, T., & Kai, K. 1985, Astrophys. J., 288, 806

Nishio, M., Yaji, K., Kosugi, T., Nakajima, H., & Sakurai, T. 1997, Astrophys. J., 489, 976

Pick, M. 1961, Ann. d'Astrophys., 24, 183

Shibasaki, K., Enome, S., Nakajima, H., Nishio, M., Takano, T., Hanaoka, Y., Torii, C., Sekiguchi, H., , Kawashima, S., Bushimata, T., Shinohara, N., Koshiishi, H., Shiomi, Y., Irimajiri, Y., Leka, K. D., & Canfield, R. C. 1994, Publ. Astron. Soc. Japan, 46, L17

Shimizu, T., Tsuneta, S., Acton, L. W., Lemen, J. R., Ogawara, Y., & Uchida, Y. 1994, Astrophys. J., 422, 906

Zirin, H. 1983, Astrophys. J., 274, 900

This preprint was prepared with the AAS LaTeX macros v5.0.

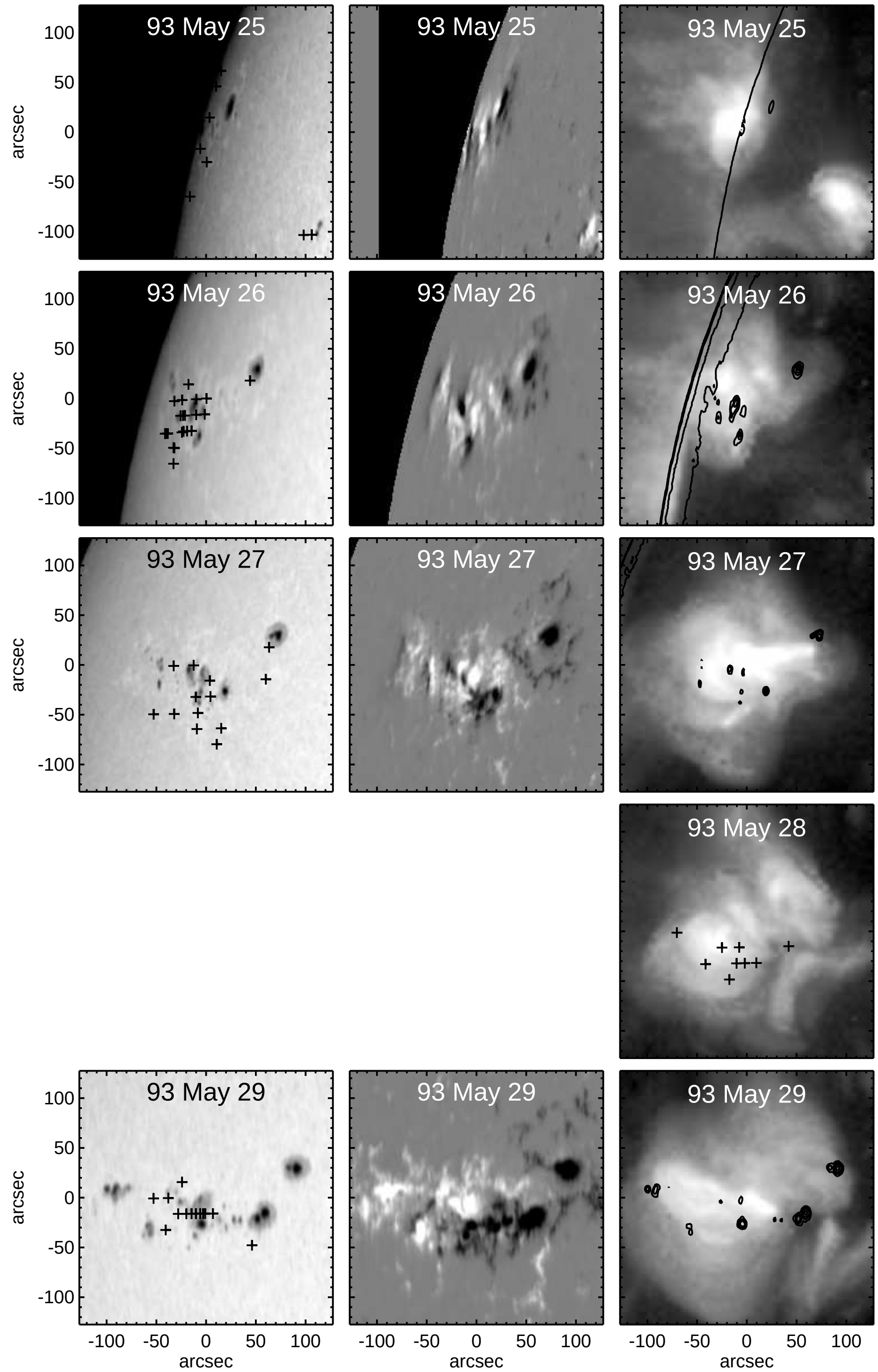

Fig. 1.— A sequence of white light images (left), KPNO magnetograms (middle), and Yohkoh-SXT images (right) for the period May 25 to June 3, 1993 (there are no KPNO data for May 28). The crosses on the white light images represent the locations of optical flares, while contours of the white light images are overplotted on the soft X-ray images to show the locations of sunspots.

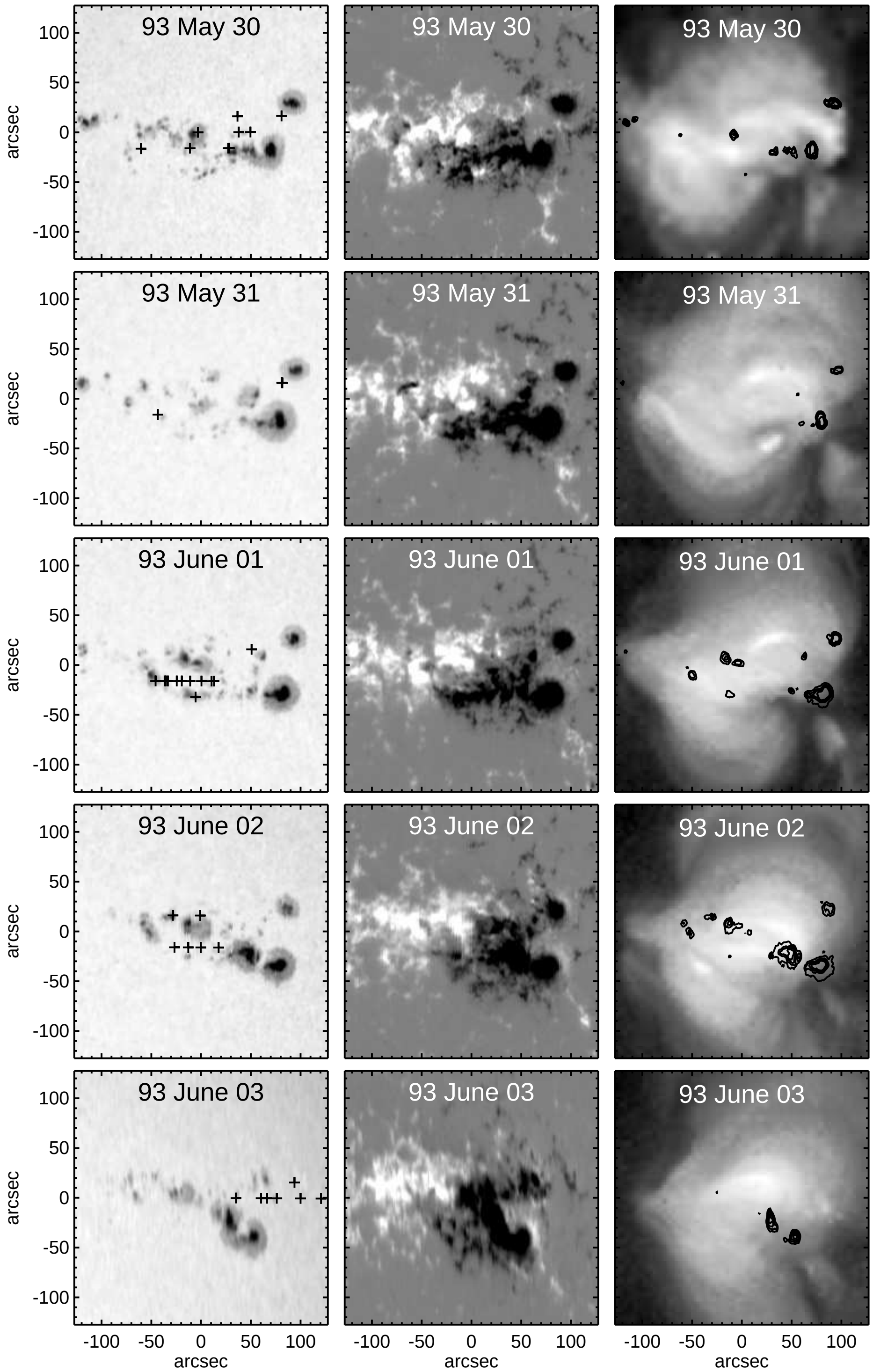

Fig. 1 (continued).—

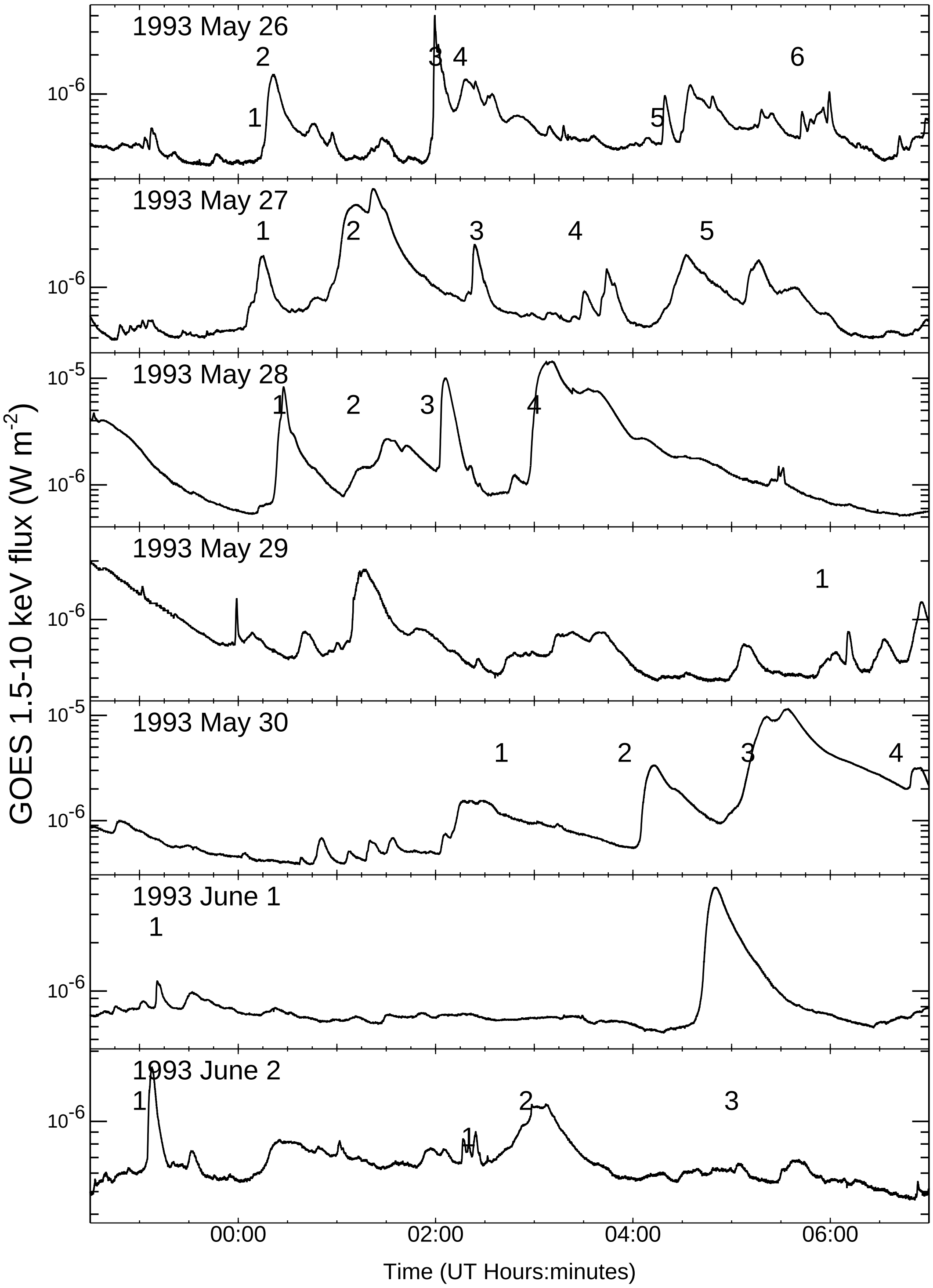

Fig. 2.— The 1.5 – 10 keV soft X–ray time profiles observed by the GOES satellite during the period May 26 - June 3, 1993 shown in Figure 1. The numbers on each panel refer to the times of 17 GHz radio bursts occurring in the target active region on each day, as shown further in Figure 3.

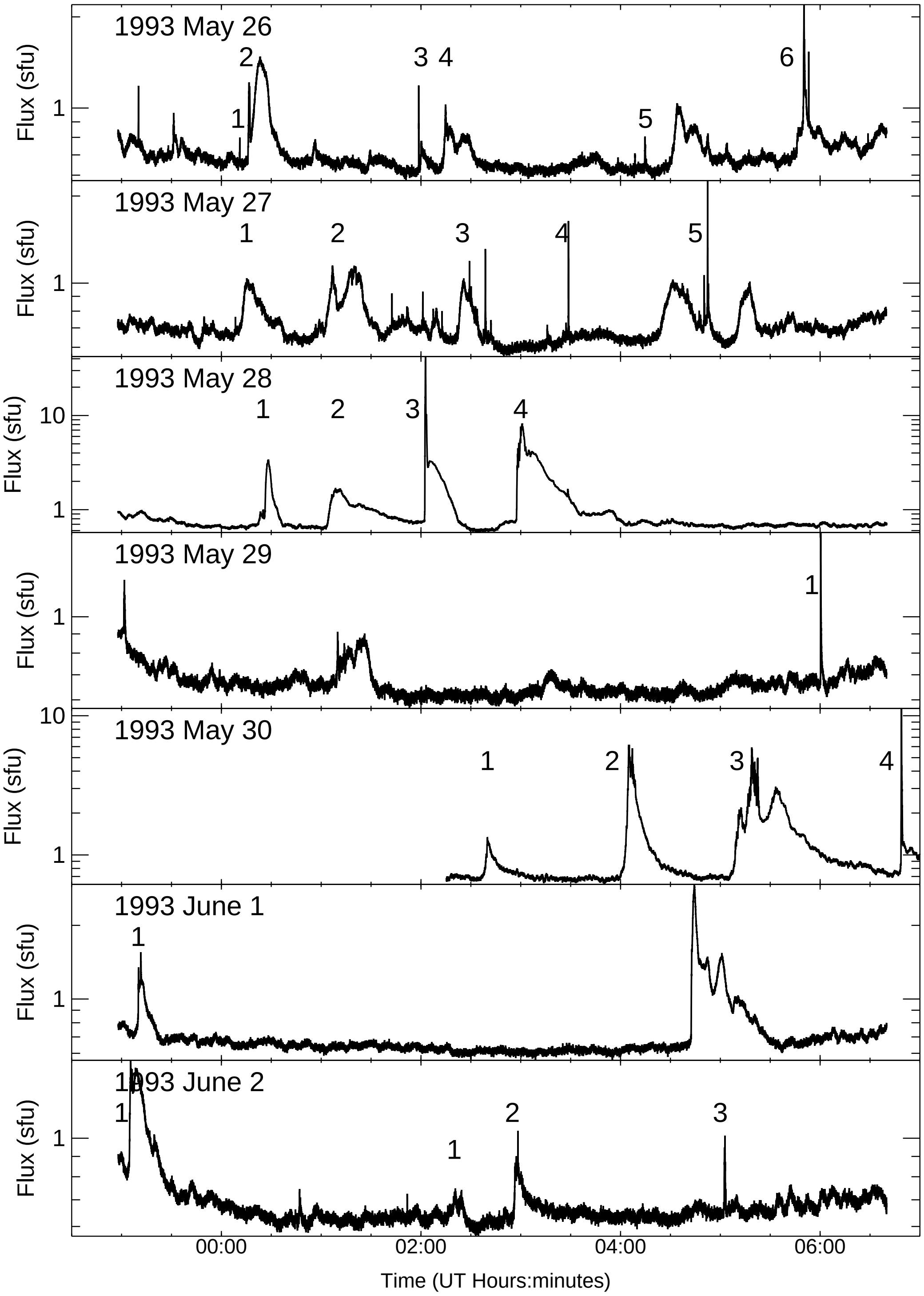

Fig. 3.— The time profiles of the bursts observed by NoRH at 17 GHz during the period May 26 - June 3, 1993. The bursts occurring in the region of interest studied in this paper are numbered 1, 2, 3, etc. as discussed in the text.

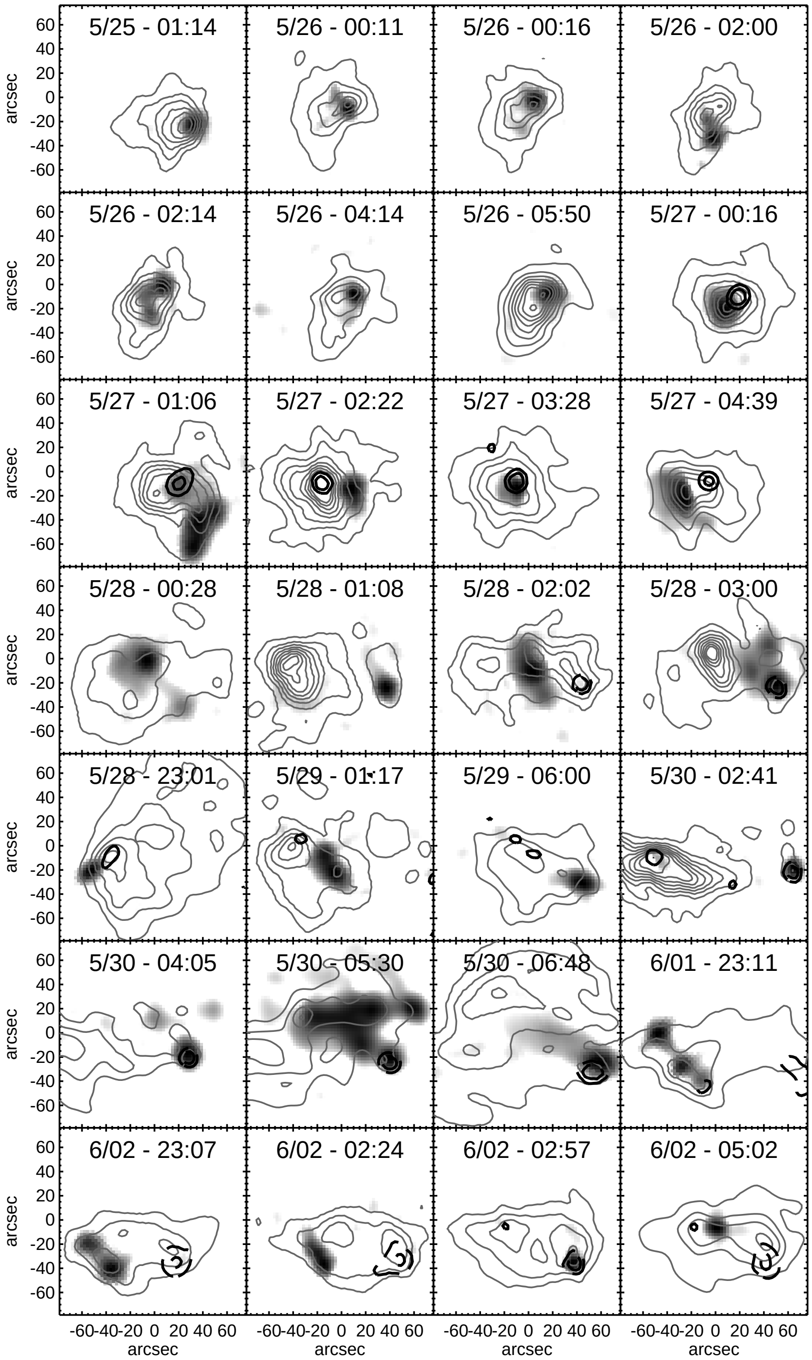

Fig. 4.— Preflare active region emission contours (grey) at 15, 30, 45, 60, 75, 90, 105 and 120×10^3 K overlaid on a greyscale representation (linear transfer function after preflare subtraction) of the subsequent flare emission for 28 flares. Thick black contours are also shown for strong circular polarization in the preflare map at 17 GHz (solid for positive circular polarization, dashed for negative circular polarization). The contours are at 30, 60 & 90 percent of the maximum circularly polarized flux in the map, but are only plotted when the maximum is well above the noise level. The fields of view are not coaligned since they are customized for each flare.

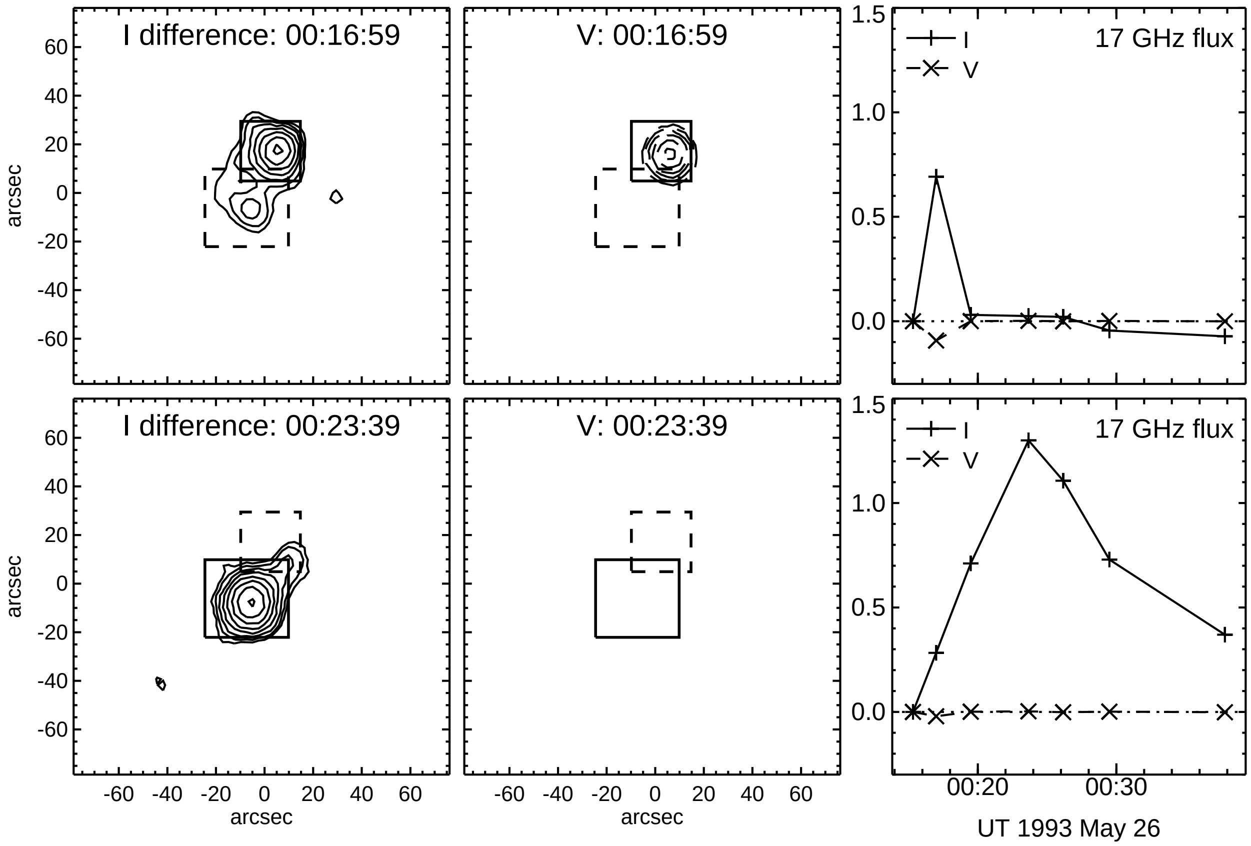

Fig. 5.— Time profiles for different components of a burst on May 26 at 00:17 UT. The left column of panels shows 17 GHz total-intensity difference images at two different times: at 00:16:59 UT in the impulsive phase, and at 00:23:39 in the gradual phase. In order to emphasize the flare emission, these images have had the preflare emission subtracted before plotting (using an image from the time corresponding to the first point in the light curve in the right panels, in this case at 00:15:20 UT). The middle column of panels presents maps of the circularly-polarized flux at the same times as the upper panels (true images, not preflare–subtracted). The boxes plotted on the images show the regions used to derive the time profiles shown in the right column of panels: in each row the box plotted with solid lines is the region used for the light curve on that row, while the boxes plotted with dashed contours are used in the other row. Both I (plus symbols) and V (cross symbols) light curves are plotted, and both have the flux in the initial image subtracted from all measurements. Contours in the images are plotted at even logarithmic intervals with 5 contours per factor of 10 increase, starting at 10^4 K in the I difference images and at 2500 K in the circularly polarized (V) maps.

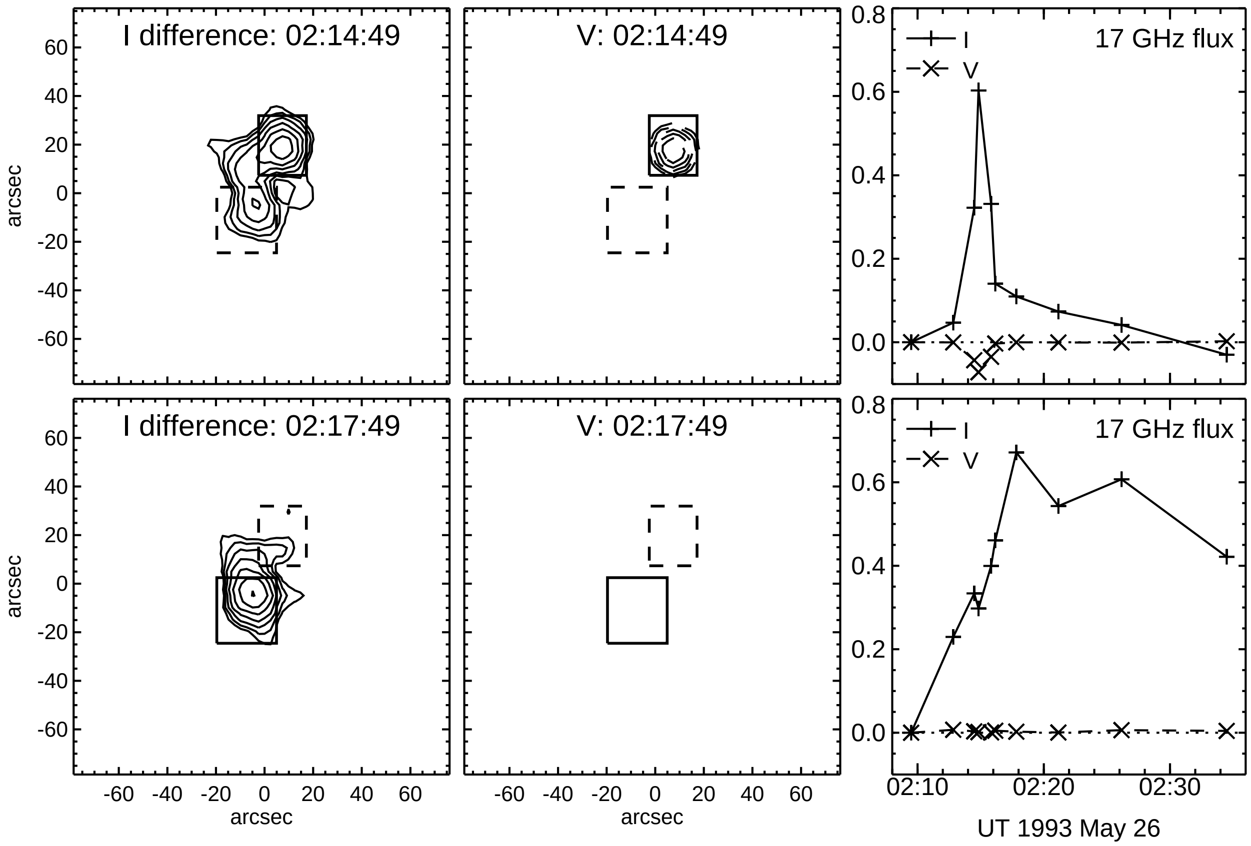

Fig. 6.— Time profiles for different components of a burst on May 26 at 02:14 UT. The left panels show 17 GHz total-intensity images at 02:14:49 UT in the impulsive phase and at 02:17:49 UT in the gradual phase. The format is similar to Figure 5.

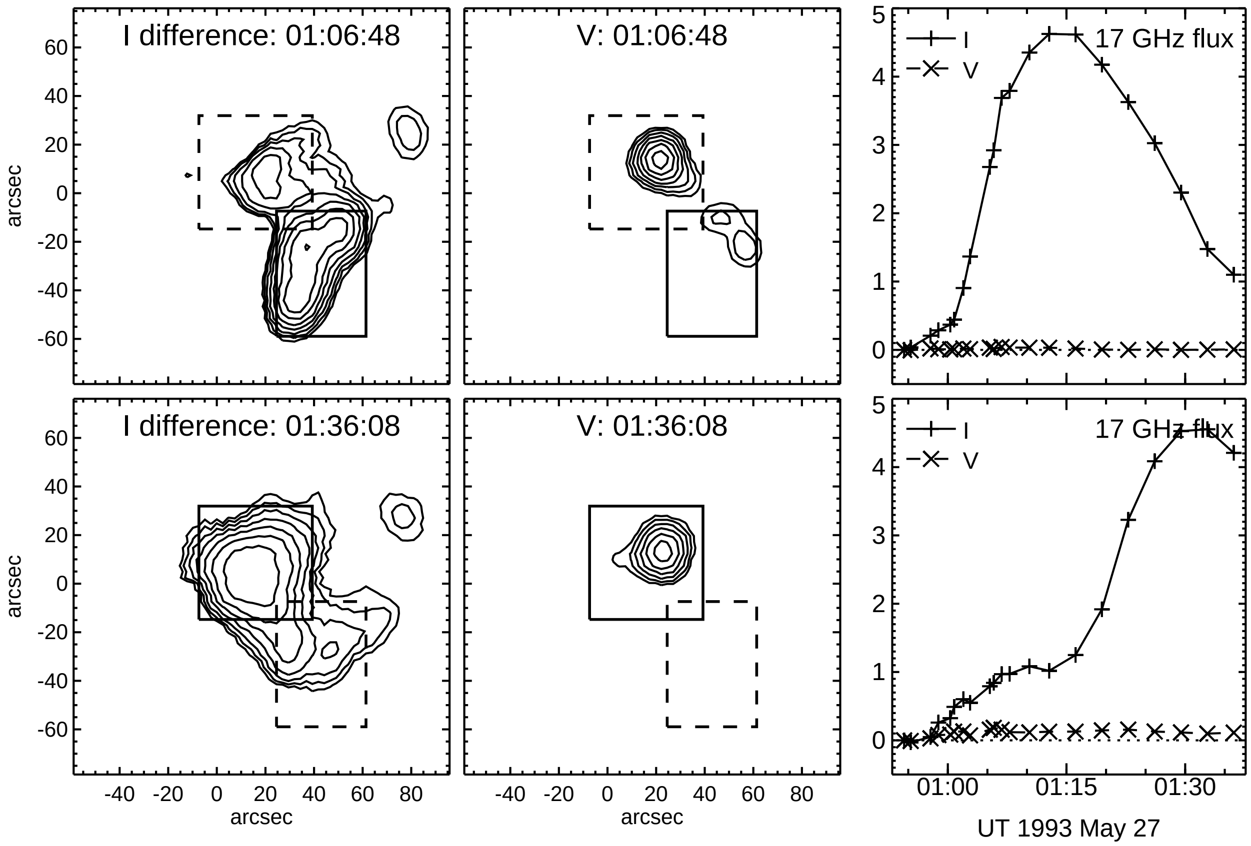

Fig. 7.— Time profiles for different components of a burst on May 27 at 00:55 UT. The left panels show 17 GHz total-intensity images at 01:06:48 UT and 01:36:08 UT. The format is similar to Figure 5.

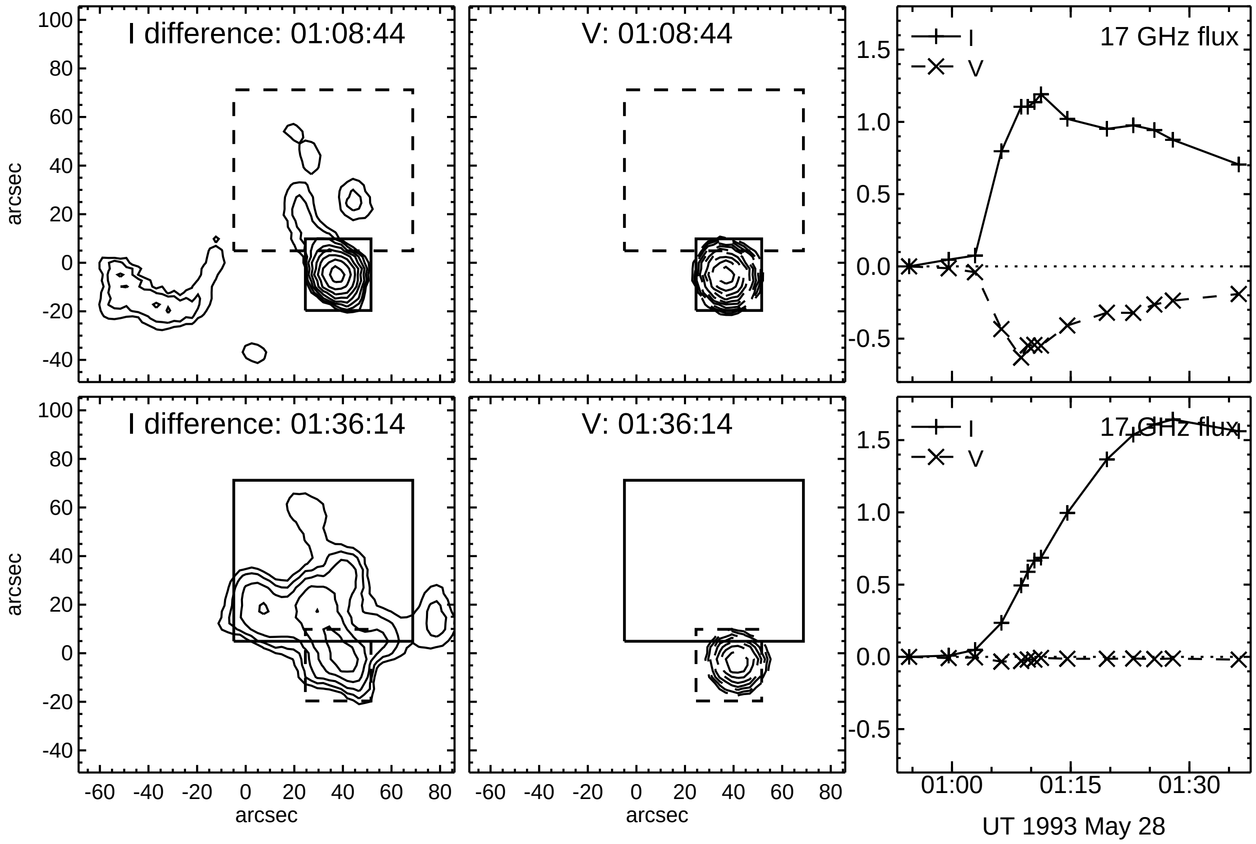

Fig. 8.— Time profiles for different components of a burst on May 28 at 01:00 UT. The left panels show 17 GHz total-intensity images at 01:08:44 UT in the impulsive phase and at 01:36:14 UT in the gradual phase. The format is similar to Figure 5.

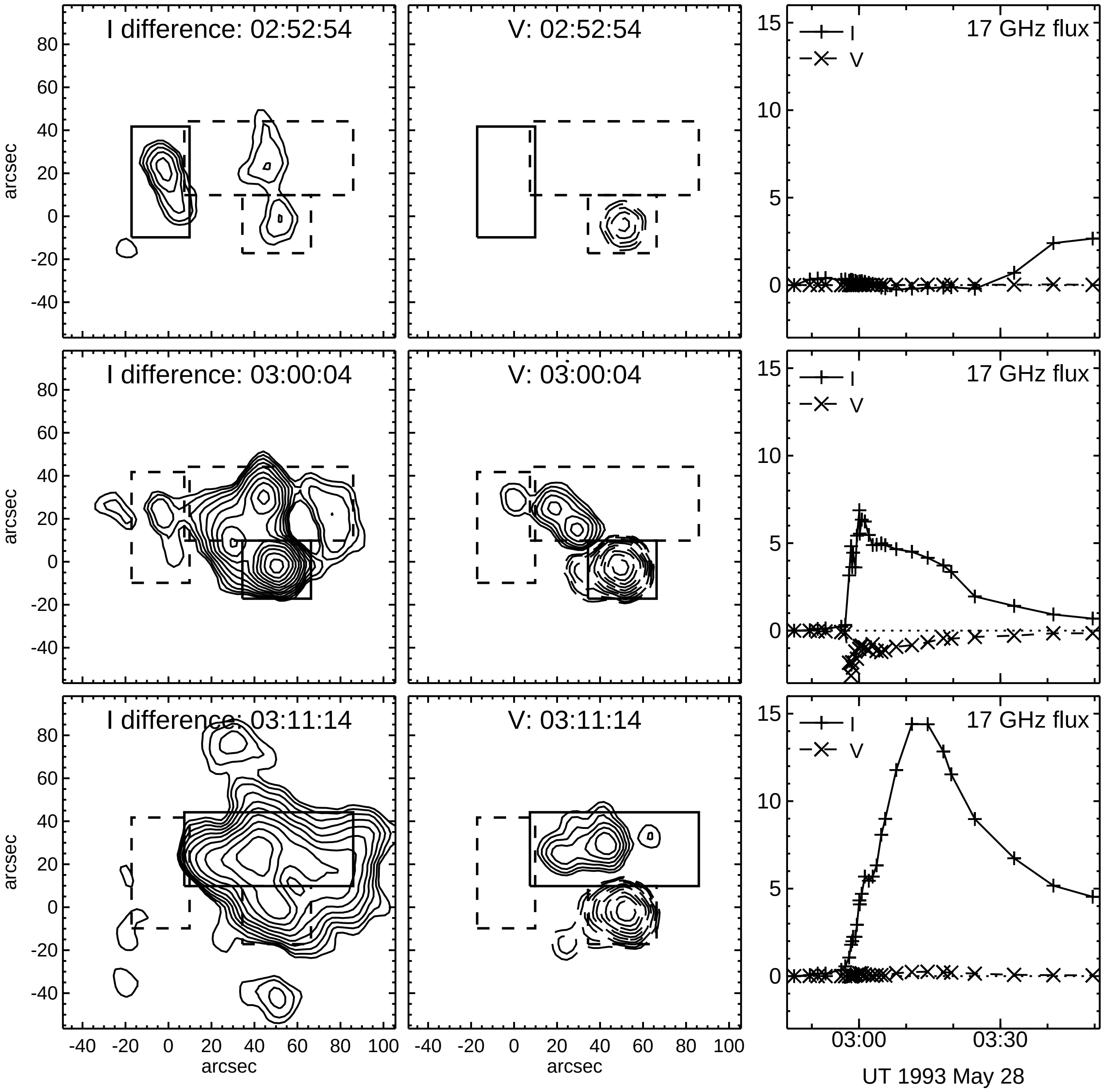

Fig. 9.— Time profiles for different components of a burst on May 28 at 03:00 UT. The left panels show 17 GHz total-intensity images at 02:52:54, 03:00:04 and 03:11:14 UT. The format is similar to Figure 5.

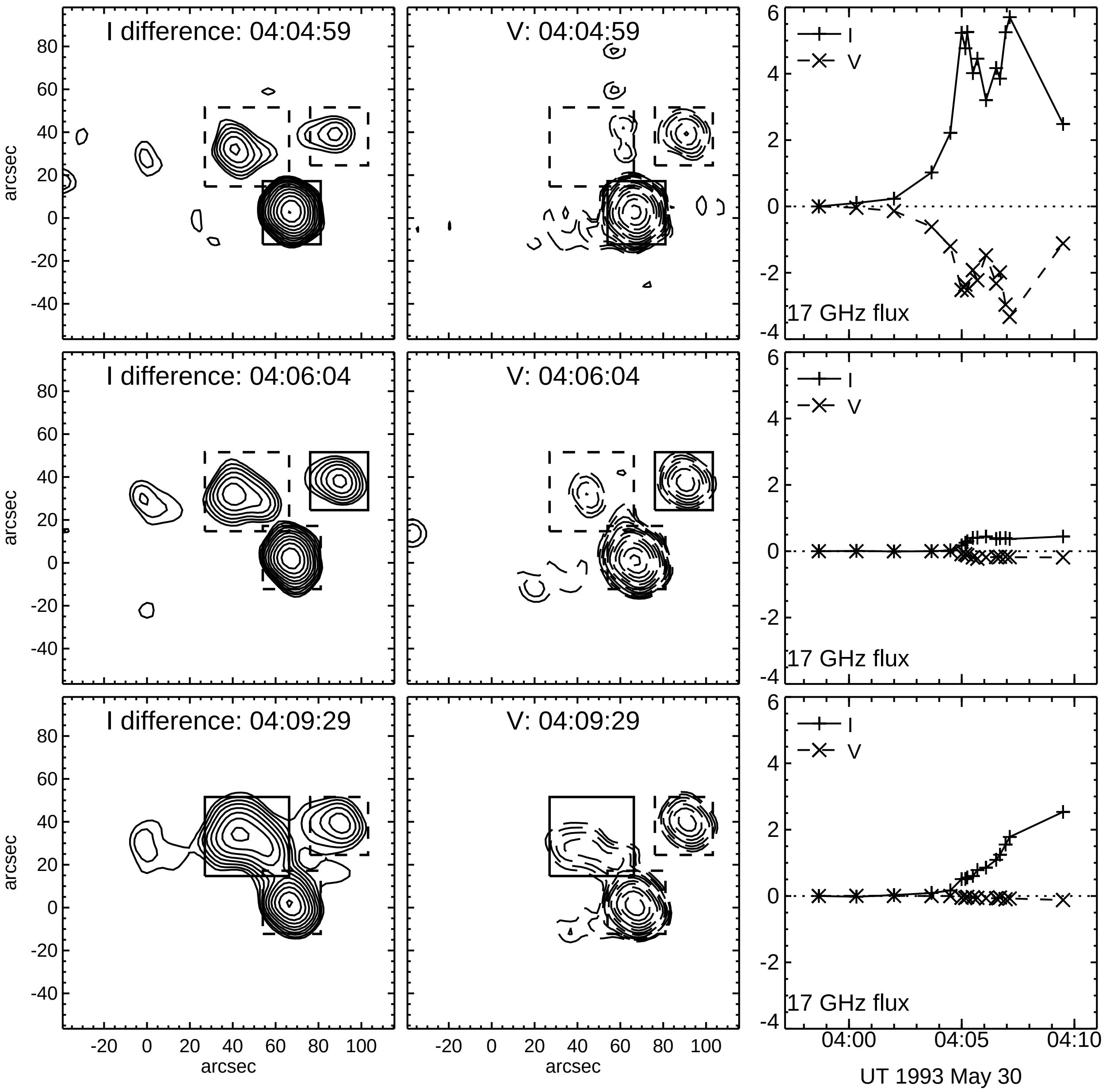

Fig. 10.— Time profiles for different components of a burst on May 30 at 04:02 UT. The left panels show 17 GHz total-intensity images at 04:04:59, 04:06:04 and 04:09:29 UT. The format is similar to Figure 5.

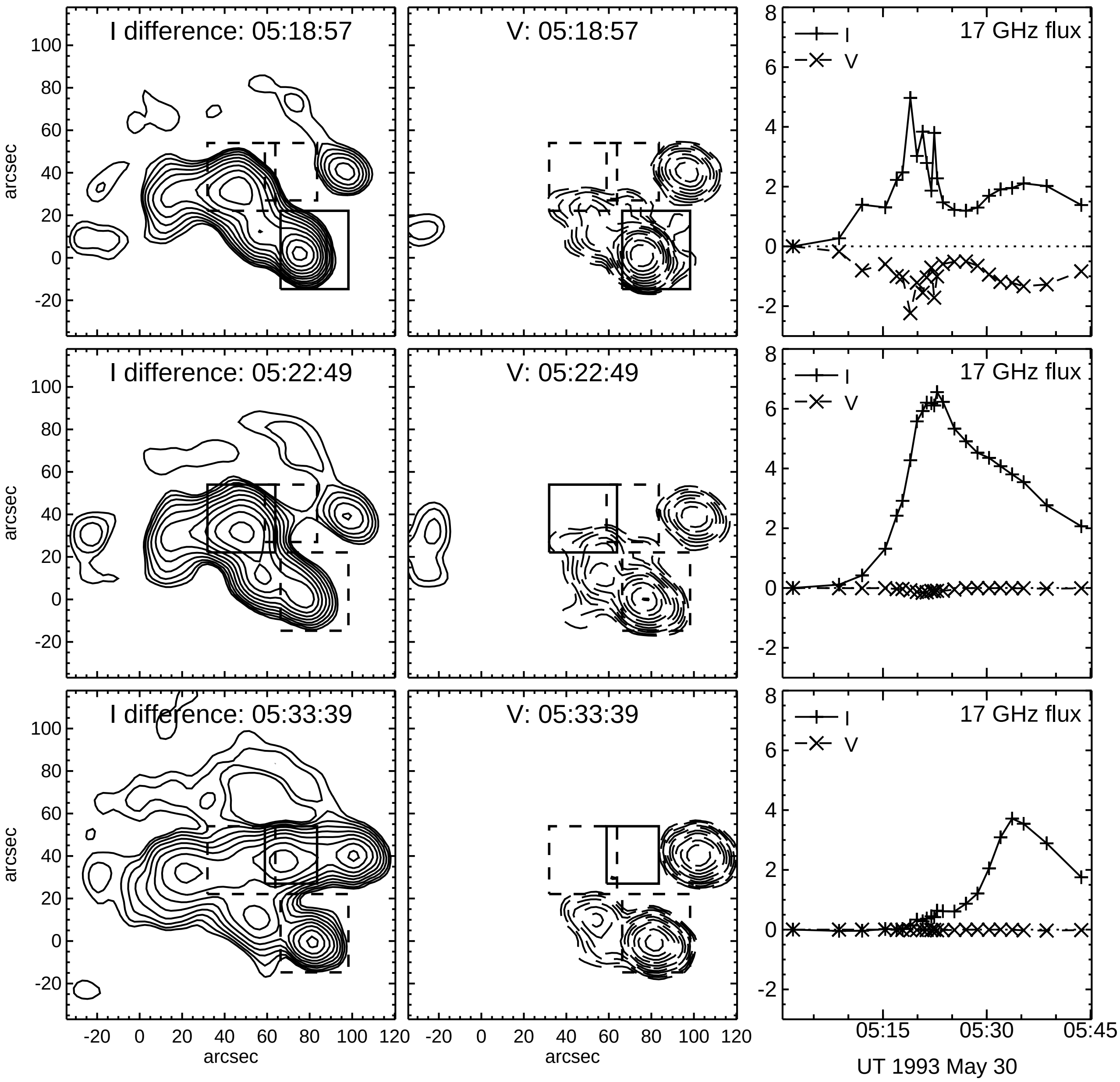

Fig. 11.— Time profiles for different components of a burst on May 30 at 05:10 UT. The left panels show 17 GHz total-intensity images at 05:18:57, 05:22:49 and 05:33:39 UT. The format is similar to Figure 5.

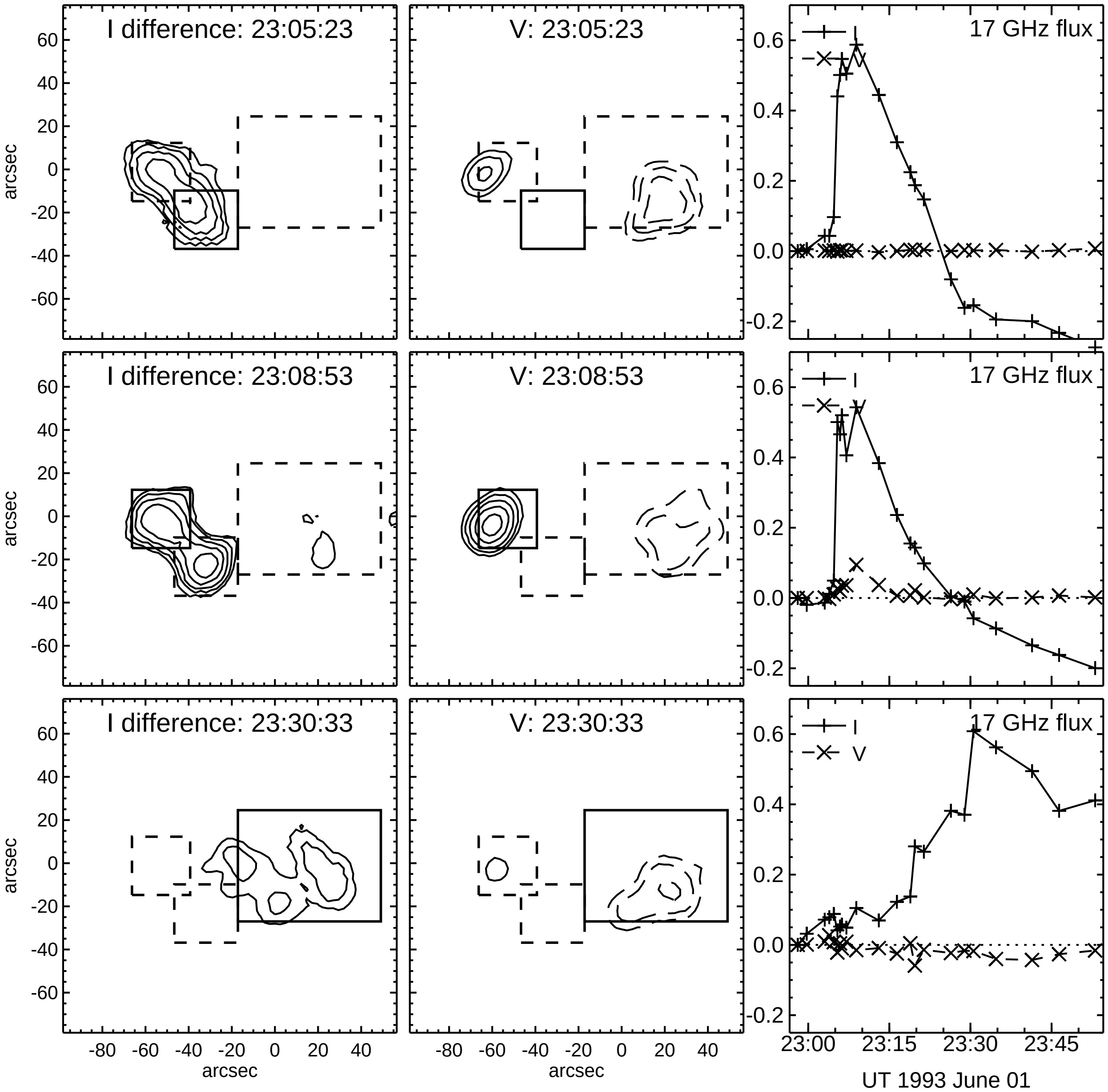

Fig. 12.— Time profiles for different components of a burst on June 01 at 23:05 UT. The left panels show 17 GHz total-intensity images at 23:05:23, 23:08:53 and 23:30:33 UT. The format is similar to Figure 5. In this event the preflare image available must contain emission from another source which is also decaying, and this causes the light curves to drop below zero in the decay phase.

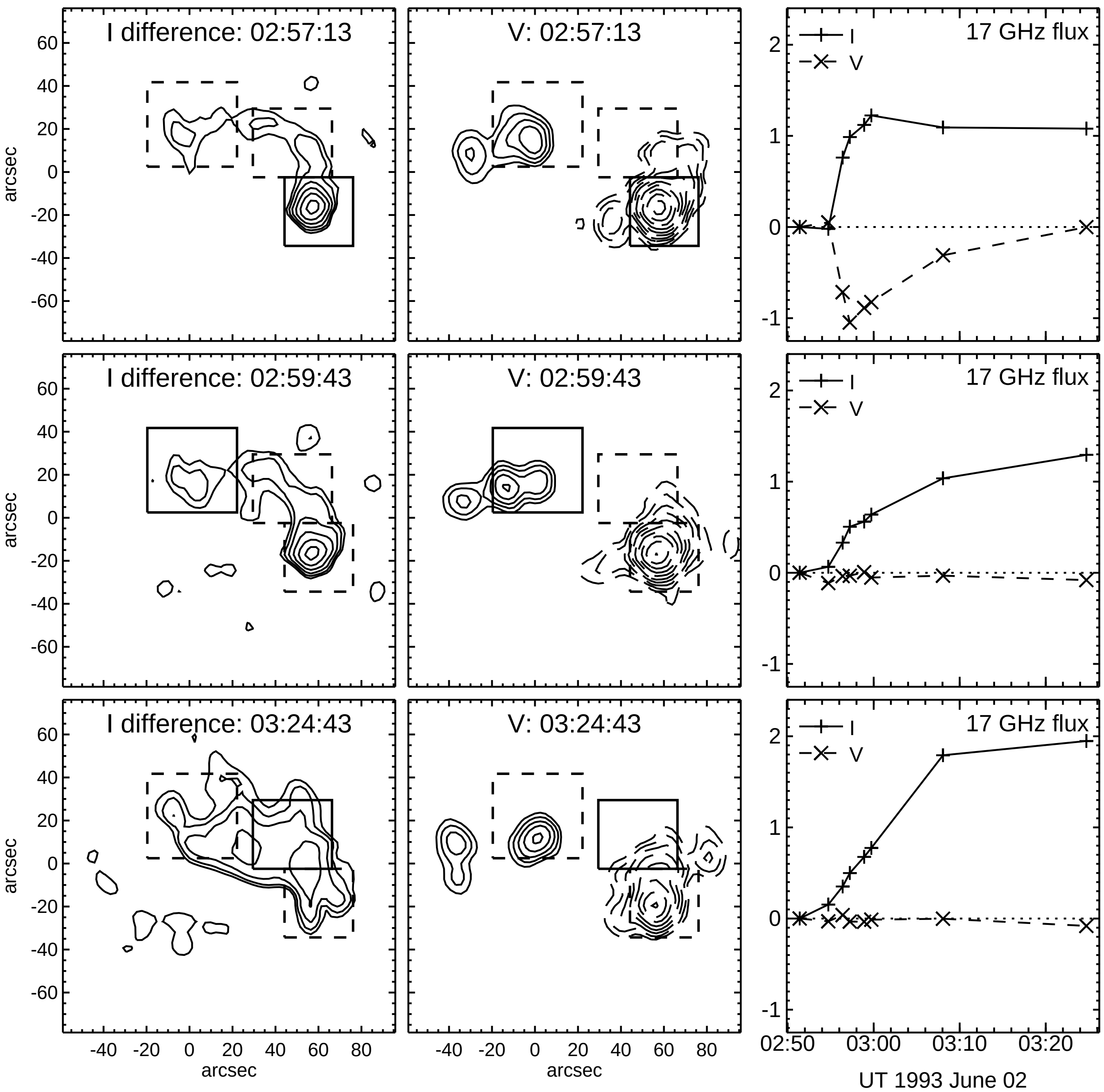

Fig. 13.— Time profiles for different components of a burst on June 02 at 02:57 UT. The left panels show 17 GHz total-intensity images at 02:57:13, 02:59:43 and 03:24:43. The format is similar to Figure 5. The three light curves correspond to sources coincident with the preflare gyroresonance source (top), the other end of the apparent loop (middle), and the center of the apparent loop (bottom), respectively.